Effects of catalyst-generated atomic hydrogen treatment on amorphous silicon fabricated by Liquid-Si printing

Hiroko Murayama[1, *], Tatsushi Ohyama[1], Akira Terakawa[1],
Hideyuki Takagishi[2, 3], Takashi Masuda[2, 4], Keisuke Ohdaira,[2, 3] and Tatsuya Shimoda[2, 3, 4]

[1]Device Solutions Center, R&D Division, Panasonic Corporation,
Moriguchi, Osaka 570-8501, Japan
[2]Japan Advanced Institute of Science and Technology,
Nomi, Ishikawa 923-1292, Japan
[3]Japan Science and Technology Agency, ALCA,
Nomi, Ishikawa 923-1292, Japan
[4]Japan Science and Technology Agency, ERATO,
Nomi, Ishikawa 923-1292, Japan
[*]E-mail: murayama.hiroko5@jp.panasonic.com

The film property distributions along the thickness direction of the catalyst-generated atomic hydrogen (Cat-H*) treatment effects on hydrogenated amorphous silicon (a-Si:H) fabricated by plasma-enhanced chemical vapor deposition (plasma-CVD) and liquid-Si printing (LSP) were systematically investigated. The a-Si:H films fabricated by LSP (L-a-Si:H) had nanosize voids; however, these films showed a decrease in void size around the surface region after Cat-H* treatment, in contrast to stable plasma-CVD films without voids. The decrease in nonaffected area by Cat-H* treatment in L-a-Si:H films improved the performance of a-Si:H solar cells with L-a-Si:H. Additionally, we achieved a 3.1% conversion efficiency for a-Si:H solar cells with L-a-Si:H as the active layer by stacking nondoped a-Si:H, fabricated by plasma-CVD, on the active layer.

1. Introduction

Hydrogenated amorphous silicon (a-Si:H) is important for Si solar cells. We have been developing a-Si:H/microcrystalline Si tandem solar cells with a high deposition rate and a high conversion efficiency for a highly cost-effective photovoltaic system.[1)-3)] We also have been developing highest performance photovoltaic heterojunctions with intrinsic thin-layer (HIT) solar cells.[3)-5)] HIT solar cells have a-Si:H as a passivation layer. The criteria for depositing high-quality a-Si:H by plasma-enhanced chemical vapor deposition (plasma-CVD) have been reported[6)-12)] and used to improve the performance of Si solar cells. However, vacuum processes, such as plasma-CVD and sputtering, were responsible for a large part of the module cost.

We are developing nonvacuum fabrication techniques to reduce the cost of vacuum processes.[1), 3), 13)] The a-Si:H fabricated by liquid-Si printing (LSP), which consists of the printing and pyrolysis of the liquid-Si material poly(dihydrosilane) (-$(SiH_2)_n$-) in nonvacuum, was expected to be applied to solar cells. The a-Si:H printed by LSP (L-a-Si:H) was previously demonstrated in TFT fabrication.[14)] It was also reported that the a-Si:H films printed by LSP showed high photoconductivities and that a-Si worked in thin-film Si solar cells.[15), 16)] In addition, we showed that the Si films and a-Si solar cells had marked photostabilities.[17)] Printed a-Si:H is a candidate for the active layer in a-Si solar cells with highly stable conversion efficiency.

The effects of atomic hydrogen treatment on a-Si:H for solar cells have been studied.[7), 15), 18)] Tsuge et al. showed that wide-gap a-Si:H of device quality can be obtained by applying the atomic hydrogen treatment by plasma-CVD to a-Si:H deposited by plasma-CVD (P-a-Si:H).[7)] The range of effects depended on the deposition and treatment temperatures. Masuda et al. reported that the photoconductivity of nondoped a-Si:H fabricated by LSP was improved by catalyst-generated atomic hydrogen (Cat-H*) from 1.5×10^{-7} to 0.9×10^{-5} S/cm, which is comparable to that of conventional nondoped a-Si:H.[15)] Thus, the atomic hydrogen treatment is valid for the improvement of a-Si:H.

For the printed a-Si:H with device grade properties, Cat-H* treatment was effective and necessary. The cost to fabricate a-Si:H by LSP and Cat-H* treatment is much lower than that to deposit P-a-Si:H. The high-quality and low-cost a-Si:H was obtained to combine LSP and Cat-H* treatment. The effects of Cat-H* treatment on the optical and electric properties and hydrogen bonding configurations of L-a-Si:H and P-a-Si:H have been investigated.[17)] Table I shows the film properties of P-a-Si:H and L-a-Si:H before and after Cat-H* treatment. Cat-H* treatment largely improved the photoconductivities and increased optical gaps of L-a-Si:H; it also increased the ratio of Si-H bonds and decreased the ratio of Si-H_2 bonds, in contrast to P-a-Si:H, in which the ratio of Si-H_2 bonds increased. These film properties were averaged in the film thickness direction; however, these films are likely to have property dis-

tributions along the thickness direction because Cat-H* treatment is carried out after fabricating a-Si:H films. In this study, we revealed the thickness direction distribution of the effects of Cat-H* treatment on L-a-Si:H. Additionally, we improved the performance of a-Si:H solar cells with L-a-Si:H.

2. Experimental procedure

a-Si:H films with thicknesses of about 150 nm were prepared by LSP and radio frequency (RF) plasma-CVD. Liquid-Si ink was a mixed solution of solvent and SiH_2 polymer (polydihydrosilane) in LSP. The polydihydrosilane ($M = 10^2$–10^7) was synthesized by the photoinduced ring-opening polymerization of cyclopentasilane (CPS).[19), 20)] The wavelength, intensity, and irradiation time were 365 nm, 15 mW/cm^2, and 10–60 min, respectively. LSP consisted of the printing and pyrolysis of Liquid-Si ink and Cat-H* treatment.[15)] The intermolecular interaction and structure of CPS and the wettability and solubility of Liquid-Si ink have been reported.[21)-24)] The Liquid-Si ink was spin-coated on glass (Corning Eagle XG) substrates at 2,000 rpm for 30 s and pyrolyzed at 430 ^{o}C for 15 min on a hot plate. Although LSP can be used to fabricate a-Si:H in a nonvacuum process, we fabricated a-Si:H by a complex three-dimensional reaction requiring a temperature above 400 ^{o}C, which was higher than 200 ^{o}C for plasma-CVD.

For Cat-H* treatment, Cat-CVD was used. The equipment used was nearly identical to that previously described.[25)] A tungsten wire with a diameter of 0.5 mm and a length of 100 cm was used as a catalyst and heated to 1850 ^{o}C. Hydrogen gas was introduced into the chamber at a flow rate of 20 sccm for 15 min. The chamber pressure and substrate temperature were maintained at 0.2 Pa and 200 ^{o}C, respectively. For comparison, L-a-Si:H and P-a-Si:H were treated with Cat-H*.

To reveal the thickness direction distribution of the hydrogen concentrations, secondary ion mass spectrometry (SIMS) was used. To detect the thickness direction distribution of voids, the Doppler broadening spectra of the positron annihilation radiation were measured as a function of the incident positron energy. The low-momentum part of the spectra was characterized by the S parameter, which was defined as the number of annihilation events over the energy range of 511 keV $\pm\Delta E$ (where ΔE = 0.76 keV). This S parameter reflects the size of vacancy-type defects.[26)-28)] The S–E curve was fitted using

$$S(E) = S_s F_s(E) + \sum S_i F_i(E), \qquad (1)$$

where $F_s(E)$ is the fraction of positrons annihilated on the surface and $F_i(E)$ is the fraction annihilated in the i^{th} layer [$F_s(E) + \sum F_i(E) = 1$]. S_s and S_i are S parameters respectively corresponding to the annihilations of positrons on the surface and in the i^{th} layer.

3. Results and discussion

3.1 Film property distributions along thickness direction of a-Si:H films

Figures 1(a) and 1(b) show the hydrogen ion intensities of P-a-Si:H and L-a-Si:H plotted against depth before and after hydrogen treatment as a result of SIMS. After hydrogen treatment, the hydrogen content of plasma-CVD films increased negligibly, while that of liquid-Si films increased greatly in the surface region. The region was around 30 nm in depth from the surface.

Figures 2(a) and 2(b) show the *S* parameter plotted against depth. In the fitting procedure for P-a-Si:H, P-a-Si:H had no voids and distribution both before and after Cat-H* treatment. In the case of L-a-Si:H, the region detected using positrons was divided into two blocks, and the width and *S* value of each block were derived by the fitting procedure. L-a-Si:H had nanosize voids except in the surface region. Additionally, the void size of L-a-Si:H decreased around the surface region after hydrogen treatment. This result corresponds to a change in hydrogen concentration.

Figure 3 shows the cross-sectional schematic for the hydrogen treatment effect on a-Si:H. Before hydrogen treatment, P-a-Si:H had no voids, while L-a-Si:H had nanosize voids. After hydrogen treatment, in P-a-Si:H, hydrogen content and the ratio of SiH_2 to SiH increased slightly. The positive correlations between the hydrogen content and the ratio of SiH_2 to SiH were represented by statistical models.[11] On the other hand, in L-a-Si:H, after hydrogen treatment, the ratio of SiH_2 to SiH decreased despite the large increase in hydrogen content around the surface of the film. Additionally, the void size decreased around the surface of the film. It was presumed that the change in hydrogen structure and the decrease in void size affect the improvement of photoconductivity. The zone affected by hydrogen treatment was about 30 nm in thickness.

3.2 Solar cell performance

Figures 4(a)-4(c) show the cross-sectional schematic of a-Si:H solar cells, and Table Ⅱ shows the I-V characteristics measured under AM 1.5, 100 mW/cm^2 light. When we fabricated an a-Si:H solar cell with a 140-nm-thick i-layer of nondoped a-Si:H by plasma-CVD and liquid-Si printing, the liquid-Si solar cell showed low performance. On the other hand, the performance of the a-Si:H solar cell with a 70-nm-thick i-layer of L-a-Si:H was improved more than that of the solar cell with the 140-nm-thick i-layer. This is because of the decrease in hydrogen treatment-nonaffected area.

Additionally, p/i buffer was inserted to suppress the plasma damage on liquid-Si-printed a-Si:H, as shown in Fig. 4(d).[16] As a result, we achieved a conversion efficiency of 1.1% with n side incidence and that of 3.1% with p side incidence. It was obvious that plasma damage by the B-doped layer deposited by plasma-CVD affected the LSP film as an active layer, and that the p/i buffer could prevent the

damage.

4. Conclusions

The thickness direction distributions of the effects of Cat-H* treatment on L-a-Si:H were systematically investigated and compared with those on P-a-Si:H. L-a-Si:H had nanosize voids, while P-a-Si:H had no voids. L-a-Si:H was strongly affected by Cat-H* treatment, whereas P-a-Si:H was only slightly affected by the treatment. Cat-H* treatment-affected zone on L-a-Si:H was 30 nm in thickness, and the hydrogen concentration increased, while the void size decreased. We improved the performance of a-Si:H solar cells with L-a-Si:H by reducing the thickness of L-a-Si:H, that is, by reducing the hydrogen treatment nonaffected area. Additionally, we achieved a conversion efficiency of 1.1% with n side incidence and that of 3.1% with p side incidence for a-Si:H solar cells with L-a-Si:H as the active layer by stacking nondoped a-Si:H as p/i buffer, fabricated by plasma-CVD, on the active layer.

Acknowledgements

This study was funded by the Japan Science and Technology Agency's Advanced Low Carbon Technology Research and Development (ALCA) and Exploratory Research for Advanced Technology (ERATO) program. The authors wish to thank Professor H. Matsumura of JAIST and Professor A. Uedono of the University of Tsukuba. The authors also wish to thank Mr. M. Matsumoto, Mr. T. Momose, and Mr. A. Sagara of Panasonic.

References

1) A. Terakawa, M. Hishida, S. Yata, W. Shinohara, A. Kitahara, H. Yoneda, Y. Aya, I. Yoshida, M. Iseki, and M. Tanaka, Proc. 26th European PV Solar Energy Conf., 2011, p. 2362.
2) Y. Aya, H. Katayama, M. Matsumoto, M. Hishida, W. Shinohara, I. Yoshida, A. Kitahara, H. Yoneda, A. Terakawa, and M. Iseki, Proc. 37th IEEE Photovoltaic Specialists Conf., 2011, p. 003577.
3) A. Terakawa, H. Murayama, Y. Naruse, H. Katayama, K. Sekimoto, S. Yata, M. Matsumoto, I. Yoshida, M. Hishida, Y. Aya, M. Iseki, M. Taguchi, and M. Tanaka, MRS Proc. **1536** (2013) 17.
4) M. Taguchi, A. Yano, S. Tohoda, K. Matsuyama, and Y. Nakamura: Proc. 39th IEEE Int. Photovoltaic Science and Engineering Conf., 2013, p. 96.
5) M. Taguchi, A. Yano, S. Tohoda, K. Matsuyama, Y. Nakamura, T. Nishiwaki, K. Fujita and E. Maruyama: Proc. 28th European Photovoltaic Solar Energy Conf., 2013, p. 748.
6) N. Nakamura, T. Takahama, M. Isomura, M. Nishikuni, K. Yoshida, S. Tsuda, S. Nakano, M. Ohnishi, and Y. Kuwano, Jpn. J. Appl. Phys. **28** 1762 (1989).
7) S. Tsuge, Y. Hishikawa, S. Okamoto, M. Sasaki, S. Tsuda, S. Nakano, and Y. Kuwano, MRS Proc. **258** (1992) 869.
8) Y. Hishikawa, S. Tsuda, K. Wakisaka, and Y. Kuwano, J. Appl. Phys. **73**, 4227 (1993).
9) S. Okamoto, Y. Hishikawa, and S. Tsuda, Jpn. J. Appl. Phys. **35**, 26 (1996).
10) T. Kinoshita, M. Isomura, Y. Hishikawa, and S. Tsuda, Jpn. J. Appl. Phys. **35**, 3819 (1996).
11) A. Terakawa and H. Matsunami, Phys. Rev. B **62**, 16808 (2000).
12) H. Rinnert and M. Vergnat, Thin Solid Films **403-404**, 153 (2002).
13) W. Shinohara, Y. Aya, M. Hishida, A. Kitahara, M. Nakagawa, A. Terakawa, and M. Tanaka, Proc. 25th European Solar Energy Conf., 2010, p. 2735.
14) T. Shimoda, Y. Matsuki, M. Furusawa, T. Aoki, I. Yudasaka, H. Tanaka, H. Iwasawa, D. Wang, M. Miyasaka, and Y. Takeuchi, Nature **440**, 783 (2006).
15) T. Masuda, N. Sotani, H. Hamada, Y. Matsuki, and T. Shimoda, Appl. Phys. Lett. **100**, 253908 (2012).
16) H. Murayama, T. Ohyama, A. Terakawa, H. Takagishi, T. Masuda, K. Ohdaira, and T. Shimoda, *to be published in* Can. J. Phys.
17) H. Murayama, T. Ohyama, I. Yoshida, A. Terakawa, T. Masuda, K. Ohdaira, and T. Shimoda, *to be published in* Thin Solid Films.
18) A. Heya, A. Masuda, and H. Matsumura, Appl. Phys. Lett. **74**, 2143 (1999).
19) E. Hengge and G. Bauer, Angew. Chem., Int. Ed. **12**, 316 (1973).

20) T. Masuda, Y. Matsuki, and T. Shimoda, Polymer **53**, 2973 (2012).
21) P. V. Dung, P. T. Lam, N. D. Duc, A. Sugiyama, T. Shimoda, and D. H. Chi, Comput. Mater. Sci. **49**, S21 (2010).
22) P. T. Lam, A. Sugiyama, T. Masuda, T. Shimoda, N. Otsuka, and D. H. Chi, Chem. Phys. **400**, 59 (2012).
23) T. Masuda, Y. Matsuki, and T. Shimoda, J. Colloid. Interface. Sci. **340**, 298 (2009).
24) T. Masuda, Y. Matsuki, and T. Shimoda: Thin Solid Films **520**, 5091 (2012).
25) A. Izumi and H. Matsumura, Jpn. J. Appl. Phys. **41**, 4639 (2002).
26) A. Uedono, K. Tsutsui, S. Ishibashi, H. Watanabe, S. Kubota, Y. Nakagawa, B. Mizuno, T. Hattori, and H. Iwai, Jpn. J. Appl. Phys. **49**, 051301 (2010).
27) A. Uedono, S. Ishibashi, K. Tenjinbayashi, T. Tsutsui, K. Nakahara, D. Takamizu, and F. Chichibu, J. Appl. Phys. **111**, 014508 (2012).
28) A. Sagara, M. Hiraiwa, A. Uedono, N. Oshima, and S. Shibata, Nucl. Instrum. Methods. Phys. Res. B **321**, 54 (2014).
29) A. Uedono and A. Sagara, private communication.
30) J. Melskens, A. H. M. Smets, S. W. H. Eijt, H. Schut, E. Bruck, and M. Zeman, J. Non-Cryst. Solids **358**, 2015 (2012).

Figure captions

Table Ⅰ. Film properties of a-Si:H fabricated by plasma-CVD and Liquid-Si printing before and after catalyst-generated atomic hydrogen treatment.

Table Ⅱ. I-V characteristics of a-Si:H solar cells measured under AM 1.5, 100 mW/cm^2 light.

Fig. 1. (Color online) Hydrogen ion intensity of a-Si:H fabricated by (a) plasma-CVD and (b) Liquid-Si printing plotted against depth as a result of SIMS. The solid line indicates the result before Cat-H* treatment and the dashed line indicates the result after the treatment.

Fig. 2. (Color online) *S* parameter of a-Si:H fabricated by (a) plasma-CVD and (b) Liquid-Si printing plotted against depth. The solid line indicates the result before Cat-H* treatment and the dashed line indicates the result after the treatment. The relationship between *S* parameter and void size is determined from Refs. 29 and 30.

Fig. 3. (Color online) Cross-sectional schematic of Cat-H* treatment effect on a-Si:H fabricated by plasma-CVD and Liquid-Si printing.

Fig. 4. (Color online) Cross-sectional schematic of a-Si:H solar cells.

Table Ⅰ

	Hydrogen treatment	Thickness (nm)	Optical gap (eV)	Conductivity (S/cm)		Photo / Dark	$[SiH_2]$ / [SiH]	Hydrogen content (at.%)
				Photo	Dark			
Plasma-CVD	Before	67	1.63	$1.1x10^{-5}$	$7.1x10^{-12}$	$1.5x10^{6}$	0.24	14.9
	After	64	1.65	$1.6x10^{-5}$	$7.1x10^{-12}$	$2.3x10^{6}$	0.44	15.6
LSP	Before	83	1.45	$5.7x10^{-8}$	$4.4x10^{-11}$	$1.3x10^{3}$	4.31	6.5
	After	80	1.51	$5.1x10^{-6}$	$3.7x10^{-11}$	$1.4x10^{5}$	2.56	7.3

Table Ⅱ

Deposition method of i-layer	i-layer thickness (nm)	V (V)	J (mA/cm^2)	FF	Eff (%)
Plasma-CVD	140	0.89	80.0	0.64	4.6
LSP	140	0.60	3.0	0.29	0.5
LSP	70	0.63	4.0	0.32	0.8

Figure 1

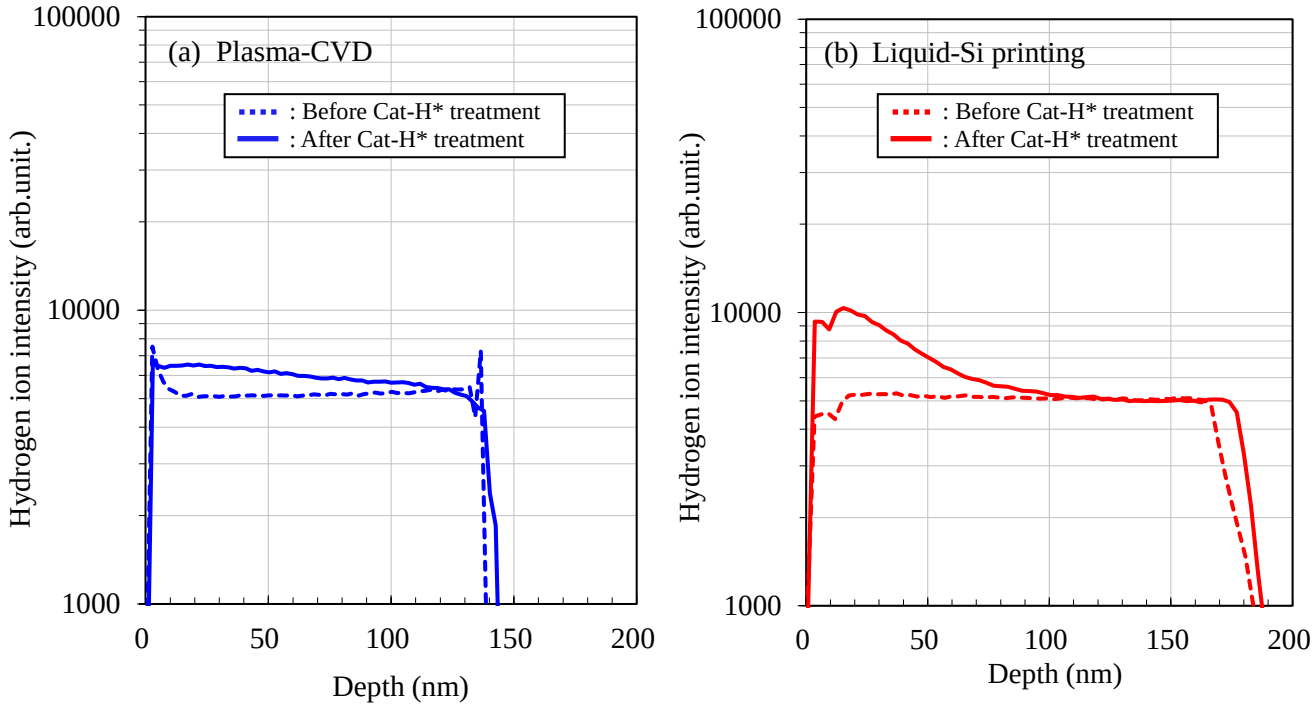
(a) Plasma-CVD
: Before Cat-H* treatment
: After Cat-H* treatment
Hydrogen ion intensity (arb.unit.)
100000
10000
1000
0
50
100
150
200
Depth (nm)
(b) Liquid-Si printing
: Before Cat-H* treatment
: After Cat-H* treatment
Hydrogen ion intensity (arb.unit.)
100000
10000
1000
0
50
100
150
200
Depth (nm)

Figure 2

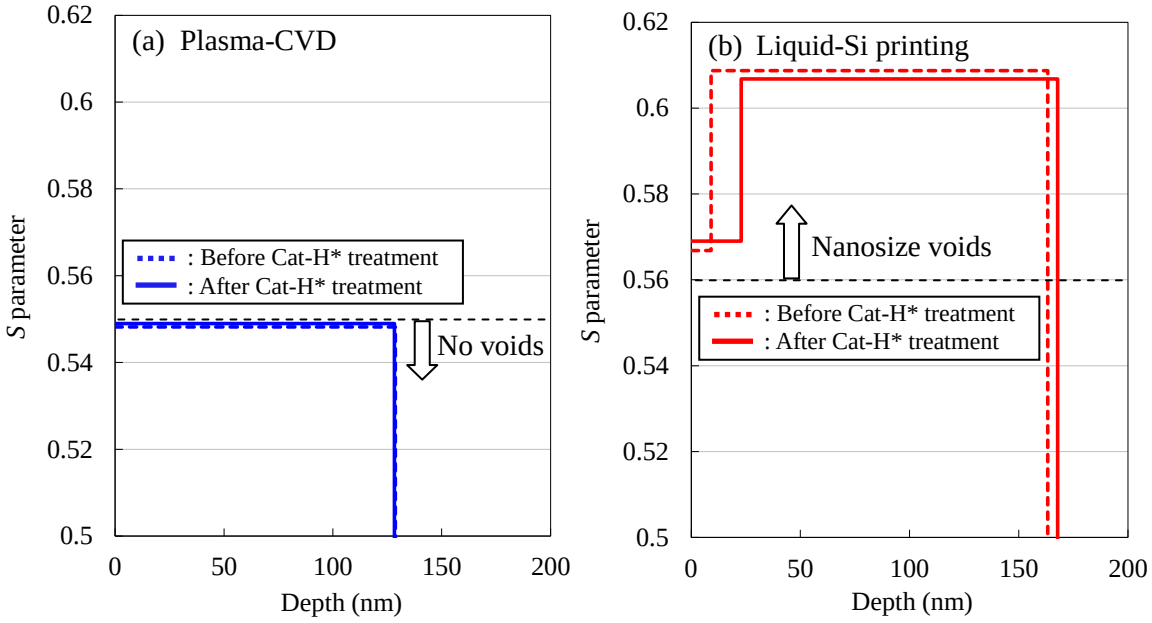
(a) Plasma-CVD
: Before Cat-H* treatment
: After Cat-H* treatment
No voids
S parameter
Depth (nm)
0.62
0.6
0.58
0.56
0.54
0.52
0.5
0
50
100
150
200
(b) Liquid-Si printing
Nanosize voids
: Before Cat-H* treatment
: After Cat-H* treatment
S parameter
Depth (nm)

Figure 3

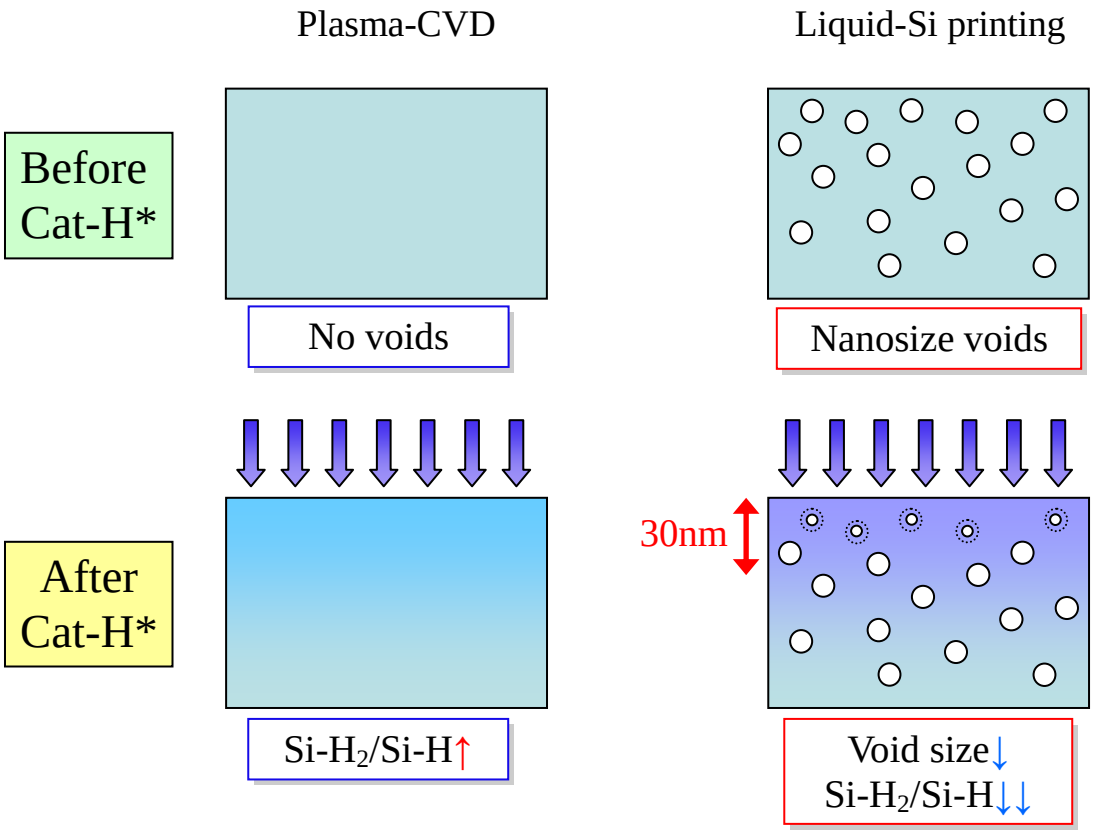
Plasma-CVD
Liquid-Si printing
Before Cat-H*
No voids
Nanosize voids
After Cat-H*
30nm
Si-H2/Si-H↑
Void size↓
Si-H2/Si-H↓↓

Figure 4

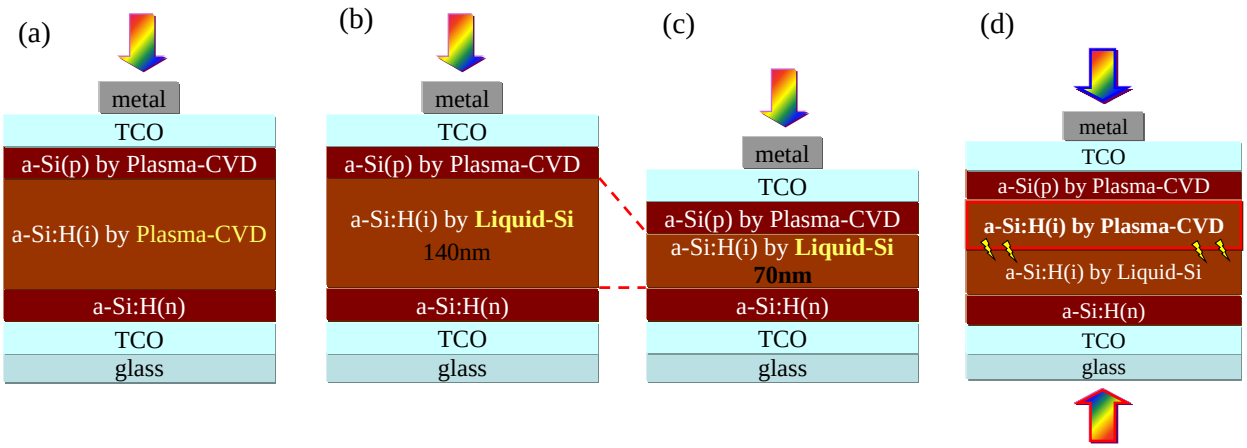
(a)
metal
TCO
a-Si(p) by Plasma-CVD
a-Si:H(i) by Plasma-CVD
a-Si:H(n)
TCO
glass
(b)
metal
TCO
a-Si(p) by Plasma-CVD
a-Si:H(i) by Liquid-Si
140nm
a-Si:H(n)
TCO
glass
(c)
metal
TCO
a-Si(p) by Plasma-CVD
a-Si:H(i) by Liquid-Si
70nm
a-Si:H(n)
TCO
glass
(d)
metal
TCO
a-Si(p) by Plasma-CVD
a-Si:H(i) by Plasma-CVD
a-Si:H(i) by Liquid-Si
a-Si:H(n)
TCO
glass